January 1, 2010

Stabilization of Thin Liquid Films Flowing over Locally Heated Surfaces via Substrate Topography

N Tiwari
JM Davis

Stabilization of thin liquid films flowing over locally heated surfaces via substrate topography

Naveen Tiwari and Jeffrey M. Davis

Citation: Physics of Fluids (1994-present) **22**, 042106 (2010); doi: 10.1063/1.3407645
View online: http://dx.doi.org/10.1063/1.3407645
View Table of Contents: http://scitation.aip.org/content/aip/journal/pof2/22/4?ver=pdfcov
Published by the AIP Publishing

Stabilization of thin liquid films flowing over locally heated surfaces via substrate topography

Naveen Tiwari and Jeffrey M. Davis[a)]
Department of Chemical Engineering, University of Massachusetts, Amherst, Massachusetts 01003, USA

(Received 27 May 2009; accepted 13 January 2010; published online 30 April 2010)

A long-wave lubrication analysis is used to study the influence of topographical features on the linear stability of noninertial coating flows over a locally heated surface. Thin liquid films flowing over surfaces with localized heating develop a pronounced ridge at the upstream edge of the heater. This ridge becomes unstable to transverse perturbations above a critical Marangoni number and evolves into an array of rivulets even in the limit of noninertial flow. Similar fluid ridges form near topographical variations on isothermal surfaces, but these ridges are stable to perturbations. The influence of basic topographical features on the stability of the locally heated film is analyzed. In contrast to its destabilizing influence on liquid films resting on heated, horizontal walls, even such nonoptimized topography is found to be effective at stabilizing the flowing film with respect to rivulet formation and subsequent rupture. Optimal topographical features that suppress variations in the free-surface shape are also determined. The critical Marangoni number at the instability threshold increases substantially with appropriate topography even for nonzero Biot numbers. An energy analysis is used to provide insight into the mechanism by which the topography stabilizes the flow. Because the stabilizing effect of the topographical features is only weakly sensitive to the governing parameters and particular temperature profile, the use of such features could be a simple alternative in applications to more complicated methods of stabilization. *© 2010 American Institute of Physics*. [doi:10.1063/1.3407645]

I. INTRODUCTION

Applications that involve thin liquid films on heated surfaces are widespread[1,2] and include falling-film evaporators, various coating and microfabrication processes, microelectromechanical systems, and microfluidic devices.[3–10] Because the surface tension of a liquid-vapor interface is a function of temperature,[11] the presence of a temperature gradient at the free-surface results in a surface tension gradient or Marangoni stress. The thermocapillary flows induced by such stresses can cause interfacial instabilities,[12,13] which have been studied extensively for uniformly heated surfaces.[1] There has been considerable theoretical work focused on thermocapillary instabilities and wave formation in thin liquid films flowing over uniformly heated surfaces.[14,15] While inertial effects are significant in these studies, instabilities also lead to interesting behavior in the lubrication[16,17] and Stokes flow[18] regimes.

Numerous recent studies also have been focused on liquid films flowing over locally heated surfaces.[19–26] In particular, for films flowing under the influence of gravity over an inclined surface containing a rectangular heater, a thermocapillary ridge develops at the upstream edge of the heater where the Marangoni stress opposes the bulk flow. This ridge breaks up into an array of regular, spanwise rivulets above a critical value of the temperature increase at the heater[27,28] (characterized by a dimensionless Marangoni parameter that quantifies the gradient in surface tension). Instability can occur even for a Biot number (Bi) of zero, in contrast to the thermocapillary instability of a thin film flowing over a uniformly heated plate.[29] The energy analysis of the governing linearized operator, which was introduced for spreading liquid films,[30–32] was subsequently interpreted[20,33] not based on the absolute energy production rates of various terms but instead on the deviation of the energy gains relative to their values for the transversely invariant, neutrally stable mode. It was revealed from this revised interpretation that the dominant instability mechanisms for zero Biot number are streamwise flow from the capillary pressure gradient (induced by the fluid ridge) and from gravity (mobility differences between slightly perturbed regions of the film).[20] For finite Biot numbers, the transverse thermocapillary flow induced by a perturbation is an additional destabilizing mechanism that dominates as Bi increases. It has been shown that even a noninertial flow is unstable.[20,21,24,25] For sufficiently thin films the behavior is universal for all values of the Reynolds number and depends only on one combined Marangoni parameter.[25,34]

It was recently shown via direct numerical simulation that appropriate modulation of the temperature profile at the free surface and thus the local surface tension gradient could be used to stabilize the film.[35] Using a feedback control to adjust the heater temperature based on continuous sensing of the free-surface temperature along a cross-section of the film, the critical Marangoni number at instability onset could be increased by up to a factor of two for $Bi=0.02$. (The suppression of inertial instabilities in falling films by Marangoni stresses from an applied temperature gradient has also been explored recently.[36]) Because such a method requires con-

[a)]Electronic mail: jmdavis@ecs.umass.edu.

tinuous monitoring of the film and local adjustment to the heater temperature, it may not be practical for some applications. It is therefore of interest to explore alternative stabilization mechanisms.

As noted by Tiwari *et al.*[24] in their presentation of the optimal perturbations to the film, the strong contribution of the film curvature to instability indicates that a suitable modification of the film curvature in the most sensitive regions might be sufficient to suppress instability. One method of modifying the film curvature is through gradients in capillary pressure induced by topographical features added to the substrate.[37–39] Noninertial coating flows over isothermal substrates with topographical features exhibit similar capillary ridges to the locally heated films but are stable to perturbations due to the restoring flow generated by the capillary pressure gradient induced by the features.[40,41] It was shown from boundary integral solutions of the unsimplified equations of Stokes flow[42] that the film closely follows the topography for capillary numbers (Ca) that are $O(1)$ or larger but a pronounced capillary ridge develops near the feature for smaller Ca. The Stokes flow results agree well with lubrication theory for $\mathrm{Ca} < 10^{-2}$. Lubrication theory was found to be accurate within this regime even for very steep features, as the slope of the free surface, and not that of the topographical feature, is the relevant constraint.[42] Comparisons to finite element solutions[43] of the full Navier–Stokes equations and to experiments[44] further confirm that lubrication theory provides surprisingly accurate results even when it is applied to situations in which its inherent restrictions are seemingly violated.

The interaction of topography with thermocapillary flow has been considered previously but not in the context of preventing rivulet instabilities in falling films. For example, Gramlich *et al.*[4] considered the use of thermocapillary flow from a series of heaters to level the capillary ridge induced by flow over a step-down feature. Gambaryan-Roisman and Stephan[45] and Helbig *et al.*[46] investigated the influence of longitudinal minigrooves aligned with the flow on the stability and heat transfer in liquid films falling as rivulets along a structured wall maintained at a constant temperature. The dynamics of a liquid film on a heated horizontal wall with topography has also been considered recently for chemically uniform[3] and heterogeneous[47] surfaces.

In this work a model is developed using lubrication theory to investigate the influence of topographical features on the stability of thin films flowing over locally heated surfaces. Representative step-down and mound features are considered. While these features are expected to be stabilizing as $\mathrm{Bi} \rightarrow 0$ due to their effect on the film curvature, they are shown to have a significant stabilizing effect even for larger Bi for which perturbations to the film induce a significant transverse thermocapillary flow. In Sec. II, the nonlinear evolution equation for the film and the linearized equation that governs the evolution of small perturbations are presented. The stabilizing effect of two-dimensional topographical features $[S(x)]$ is explored in Sec. III A. In particular, step-down and mound features are considered, and the depth, width, and steepness of the features are varied. Optimal features that eliminate variations in the free-surface shape are also computed. Results of an energy analysis of the governing linearized operator are shown in Sec. III B. Conclusions are presented in Sec. IV.

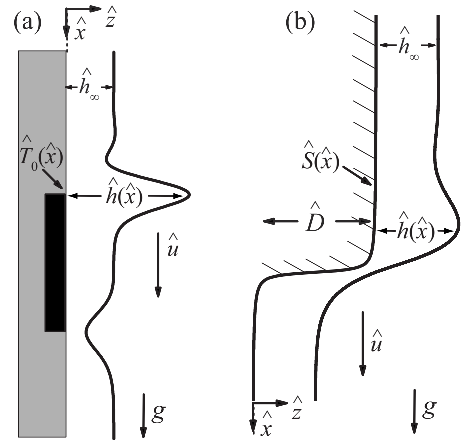

FIG. 1. (a) Thin liquid film flowing over a heater. The Marangoni stress at the upstream edge of the heater opposes the gravitational flow, which leads to the formation of a fluid ridge. (b) Isothermal liquid film flowing over step-down topography. The fluid ridge forms in response to the capillary pressure gradient induced by the topography.

II. PROBLEM FORMULATION

Consider a thin liquid film of density ρ and viscosity μ flowing under the influence of gravity along a vertical substrate, as shown in Fig. 1(a). The steady unperturbed film has local thickness $\hat{h}(\hat{x})$, and the fluid is incompressible. Imbedded in the substrate is a heater of finite width in the streamwise direction, which is modeled as a prescribed temperature variation, $\hat{T}_0(\hat{x})$, along the substrate. The film flows in the $\hat{x}$-direction, $\hat{z}$ is normal to the substrate, and $\hat{y}$ is the transverse coordinate in the plane of the substrate. The film has a constant thickness $\hat{h}_\infty$ far upstream of the heater, which corresponds to a constant flow rate. The velocity field in the liquid is $\hat{\boldsymbol{u}}$. As shown in Fig. 1(a), a pronounced thermocapillary ridge forms at the upstream edge of the heater where a Marangoni stress opposes the bulk flow. This ridge is unstable to transverse perturbations above a critical value of the Marangoni parameter.[24]

Liquid films flowing over surfaces with topographical features also exhibit capillary ridges,[39] as shown in Fig. 1(b). The film and substrate are at the ambient temperature, and the profile of the topography is $\hat{S}(\hat{x})$, with characteristic amplitude $\hat{D}$. Such ridges that form in response to step-down, mound, and trench features are stable to transverse perturbations.[40,41]

The nonlinear evolution equations for the local thickness of liquid films flowing over surfaces with nonuniform heating,[20] topographical features,[38] and both types of heterogeneity[4,47] have been derived previously using a long-wave lubrication analysis, so only a brief derivation is given here. A linear variation in surface tension with temperature is assumed, $\gamma(\hat{T}) = \gamma_0 - \gamma_T(\hat{T} - \hat{T}_\infty)$, where $\gamma_T = \partial\gamma/\partial\hat{T} > 0$ and γ_0 is the surface tension at the ambient temperature $\hat{T}_\infty$. The surface tension is treated as constant at $\gamma = \gamma_0$ in the normal stress balance, which simplifies at leading order to the specification of the capillary pressure, $\hat{p}_{\text{cap}}=-\gamma_0\hat{\nabla}^2(\hat{h}+\hat{S})$. The tangential stress balance simplifies to $\partial\hat{\boldsymbol{u}}/\partial\hat{z}=1/\mu\hat{\nabla}\gamma=-(\gamma_T/\mu)\hat{\nabla}\hat{T}^i$ at $\hat{z}=\hat{h}+\hat{S}$, where $\hat{T}^i\equiv\hat{T}(\hat{x},\hat{y},\hat{z}=\hat{h}+\hat{S})$ is the temperature at the liquid-gas interface. Integrating the simplified momentum equation twice and applying the no-slip condition at the substrate and the tangential stress balance yields an expression for the velocity field,

$$\hat{\boldsymbol{u}}=\left[\frac{\rho g}{\mu}\boldsymbol{e}_x+\frac{\gamma_0}{\mu}\hat{\nabla}\hat{\nabla}^2(\hat{h}+\hat{S})\right][\hat{h}(\hat{z}-\hat{S})-(\hat{z}-\hat{S})^2/2]-\frac{\gamma_T}{\mu}(\hat{z}-\hat{S})\hat{\nabla}\hat{T}^i. \tag{1}$$

As in related analyses,[4] it is assumed that the viscosity is constant.

The total flux in the film is $\hat{\boldsymbol{Q}}=\int_{\hat{S}}^{\hat{S}+\hat{h}}\hat{\boldsymbol{u}}d\hat{z}$. The flux is related to the local film thickness $\hat{h}$ through mass conservation for the incompressible fluid, $\hat{h}_{\hat{t}}=-\hat{\nabla}\cdot\hat{\boldsymbol{Q}}$. In dimensional form, the resulting evolution equation for the film thickness is

$$\frac{\partial\hat{h}}{\partial\hat{t}}+\frac{1}{\mu}\hat{\nabla}\cdot\left\{[\rho g\boldsymbol{e}_x+\gamma_0\hat{\nabla}\hat{\nabla}^2(\hat{h}+\hat{S})]\frac{\hat{h}^3}{3}-\gamma_T\frac{\hat{h}^2}{2}\hat{\nabla}\hat{T}^i\right\}=0. \tag{2}$$

The first term in brackets corresponds to flow due to gravity, the second term corresponds to the capillary pressure gradient from the curvature of the film and the topography, and the final term corresponds to the linear shear flow induced by the Marangoni stress.

To convert Eq. (2) to dimensionless form, the coordinates are scaled as $\hat{x},\hat{y},\hat{z}=(l_cx,l_cy,\hat{h}_\infty z)$, where l_c is the dynamic capillary length given by $l_c=\hat{h}_\infty(3\text{Ca})^{-1/3}$. The capillary number is $\text{Ca}=\mu U_c/\gamma_0$, and the characteristic velocity of the film corresponds to the Nusselt solution, $U_c=\rho g\hat{h}_\infty^2/(3\mu)$. Attention is restricted to topographical features with height comparable to the film thickness, so both are scaled with $\hat{h}_\infty$, $(\hat{h},\hat{S})=\hat{h}_\infty(h,S)$, which corresponds to the distinguished limit $\hat{h}_\infty/l_c\sim\hat{D}/l_c\ll 1$, where $\hat{D}$ is the amplitude of the topography. The temperature is written in dimensionless form as $T=(\hat{T}-\hat{T}_\infty)/\Delta\hat{T}$, where $\Delta\hat{T}$ corresponds to the maximum temperature increase at the heater, $\max[\hat{T}_0(x)-\hat{T}_\infty]$. When $S_x\neq 0$, neglecting the hydrostatic component of gravity along the sides of the topographical feature requires $\text{Ca}^{2/3}|S_x|\ll 1$. With $\text{Re}=\rho\hat{h}_\infty U_c/\mu$, the Reynolds number, Eq. (2) is strictly valid for $\text{Ca}^{1/3}\,\text{Re}\ll 1$, $\text{Ca}^{1/3}|S_x|\ll 1$, and $\text{Ca}^{2/3}D/\delta^2\ll 1$, where D and δ characterize the dimensionless amplitude and steepness of the topography introduced in Sec. III.[39] It has been shown, however, through comparisons to Stokes flow[42] and finite element[43] solutions and experiment[43,44] that the evolution equation derived using lubrication theory [Eq. (2)] is a valid approximation for small Ca (approximately smaller than 10^{-2}) even for steep features. While the *a priori* lubrication-theory estimate of the interface slope is based on the topography slope, Stokes flow solutions show *a posteriori* that the streamwise variation is much smaller than this estimate even for sharp topographies,[42] which allows the constraints on Eq. (2) to be relaxed significantly in practice. Introducing the above scalings yields the dimensionless evolution equation for the film thickness,

$$\frac{\partial h}{\partial t}+\nabla\cdot\{[\boldsymbol{e}_x+\nabla\nabla^2(h+S)]h^3-Mh^2\nabla T^i\}=0, \tag{3}$$

where $M=3^{1/3}\gamma_T\Delta\hat{T}/(2\gamma_0\text{Ca}^{2/3})$ is the Marangoni parameter that characterizes the relative magnitude of the gradient in surface tension.

The boundary conditions for Eq. (3) correspond to a uniform film away from the heater and topography,

$$h\to 1,\quad h_x\to 0\quad\text{as}\quad x\to\pm\infty. \tag{4}$$

For numerical computations, these boundary conditions were implemented in a finite domain at $x=-L_1$ and $x=L_2$, where L_1 and L_2 increased until there was no effect on the results, which typically required $L_2+L_1>L$, with $L\geq 50$ for the base states.

Subject to a prescribed temperature at the substrate, $\hat{T}(\hat{x},\hat{y},\hat{z}=\hat{S}(\hat{x}))=\hat{T}_0(\hat{x})$, and Newton's law of cooling at the liquid-gas interface, the dimensionless temperature at the free surface is[24]

$$T^i=\frac{T_0(x)}{1+\text{Bi}h}, \tag{5}$$

where $\text{Bi}=k_{\text{conv}}\hat{h}_\infty/k_{\text{th}}$ is the Biot number, k_{th} is the thermal conductivity of the liquid, and k_{conv} is the convective heat transfer coefficient in the gas. This equation is valid if $\text{Pe}\,\text{Ca}^{1/3}\ll 1$, where $\text{Pe}=U_c\hat{h}_\infty/\alpha_{\text{th}}$ is the Peclet number and α_{th} is the thermal diffusivity of the liquid at the ambient temperature. Further details on the reduction of the Navier–Stokes and energy equations can be found in previous work.[24,47]

For consistency with some previous studies of instabilities in thin liquid films flowing over locally heated, planar surfaces,[24–26] the temperature profile along the substrate is modeled as

$$T_0(x)=0.5[\tanh(\omega x+4)-\tanh(0.5x-4)], \tag{6}$$

where the parameter ω controls the steepness of the temperature increase at the upstream edge of the heater. A typical film profile for such a temperature variation is shown in Fig. 1(a).

To specify representative values of the governing parameters, consider water at 20 °C with $\gamma_0=0.073$ N/m, $\gamma_T=1.9\times 10^{-4}$ N/(m·K), and $\rho=988$ kg/m^3. For $\hat{h}_\infty=50$ μm, $\text{Ca}=1.1\times 10^{-4}$ and $M\approx 16$ for $\Delta\hat{T}=20$ °C. For $\hat{h}_\infty=20$ μm, $\text{Ca}=1.8\times 10^{-5}$ and $M\approx 22$ for $\Delta\hat{T}=8$ °C. Also consider a silicone oil of modest viscosity and relatively high density at

20 °C with $\gamma_0=0.02$ N/m, 9, $\rho=940$ kg/m^3, and $\mu=5\times10^{-3}$ kg/(m s). For $\hat{h}_\infty=50$ μm, Ca$=3.8\times10^{-4}$ and $M\approx11$ for $\Delta\hat{T}=20$ °C. For $\hat{h}_\infty=20$ μm, Ca$=6.1\times10^{-5}$ and $M\approx19$ for $\Delta\hat{T}=10$ °C. The parameter values chosen below are thus reasonable for modest heating of thin films.

A. Base profiles

The steady two-dimensional base profile is found by seeking solutions of the form $h(x,y,t)=h_0(x)$. Making this substitution into Eq. (3), integrating once, and applying the boundary conditions in Eq. (4) yield

$$h_{0xxx}+S_{xxx}=MT_x^i/h_0+h_0^{-3}-1. \tag{7}$$

The base states were computed for a finite domain, $x\in[-L_1,L_2]$ with $h_0(x=-L_1)=1$, $h_{0x}(x=-L_1)=0$, and $h_{0x}(x=L_2)=0$. Finite element computations were performed using MATLAB 6.1 and COMSOL 3.3 to determine the base profiles for a prescribed temperature field $T_0(x)$ at the solid surface and given topography $S(x)$ using a modified damped Newton method[48] to solve Eq. (7). The base profile was calculated for small values of M and D based on an initial guess value of $h_0=1$, and a continuation method[49] was used to extend the solution to larger values of these parameters. Quadratic elements were used, and the evolution equation was solved as two coupled equations by introducing an additional variable for the (linearized) curvature of the interface. Additional computations were performed by evolving the one-dimensional version of Eq. (3) in time via the method of lines[50] and the implicit DASPK solver[51,52] until a steady profile was obtained, with a unit height profile used for the initial condition. The results were identical to the solution of Eq. (7) as an ODE but can also provide some dynamical information about the stability of the solutions. The accuracy of the solution method was assessed by checking convergence after mesh refinement, varying the domain length, and examining the invariance of $\int_{-\infty}^{\infty}[MT_x^i/h_0+(1-h_0^3)/h_0^3]dx=0$. This property is guaranteed from Eq. (7) and its boundary conditions in Eq. (4), and the value of this integral was always less than 10^{-9}. Typically, about 2000 mesh points were used for the computations, with local refinement of the mesh around the regions with steep gradients in the temperature, topography, and free-surface shape.

B. Linear stability

To investigate the stability of these two-dimensional solutions to perturbations that vary in the transverse direction, the film thickness is perturbed as $h(x,y,t)=h_0(x)+\epsilon G(x,t)\exp(iqy)$, with $\epsilon\ll1$ and q as the transverse wave number of the perturbation. Upon substitution into Eq. (3) and collecting $O(\epsilon)$ terms, the linearized equation governing the evolution of perturbations is obtained,

$$\frac{\partial G}{\partial t}=\sum_{i=0}^{i=4}\mathbb{L}_iG^{(i)}, \tag{8}$$

where $G^{(i)}$ represents the ith derivative of G. The coefficients of the linear operator are

$$\begin{aligned}
\mathbb{L}_0&=-[3(h_0^2(1+h_{0xxx}+S_{xxx}))_x-2M(T_{0x}^ih_0)_x\\
&\quad-M(T_{1x}^ih_0)_x+q^2MT_1^ih_0^2+q^4h_0^3],\\
\mathbb{L}_1&=-[3h_0^2(1+h_{0xxx}+S_{xxx})-3q^2h_0^2h_{0x}-2MT_{0x}^ih_0\\
&\quad-MT_{1x}^ih_0-M(T_1^ih_0^2)_x],\\
\mathbb{L}_2&=-[-2q^2h_0^3-Mh_0^2T_1^i],\\
\mathbb{L}_3&=-3h_0^2h_{0x},\\
\mathbb{L}_4&=-h_0^3.
\end{aligned} \tag{9}$$

Due to the perturbation in h, the interfacial temperature profile becomes $T^i=T_0^i+\epsilon G(x,t)\exp(iqy)T_1^i$, where $T_0^i(x)=T_0/(1+\text{Bi}h_0)$ and $T_1^i(x)=-\text{Bi}T_0/(1+\text{Bi}h_0)^2$. Equation (8) is solved subject to the boundary conditions

$$G\quad\text{bounded as}\quad x\to\pm\infty, \tag{10}$$

which allows for both discrete modes and the leading continuous mode that asymptotes to a constant value as $x\to\pm\infty$.[24] These boundary conditions can be implemented numerically as $G_x=0$ and $G_{xxx}=0$ at $x=-L_1$ and $x=L_2$.

When discretized in space using fourth-order centered finite differences, Eqs. (8) and (10) yield a linear system of equations that can be written in vector form as

$$\frac{\partial\mathbf{G}}{\partial t}=\mathbf{A}\mathbf{G}, \tag{11}$$

where $\mathbf{A}$ is an autonomous matrix and $\mathbf{G}$ is the discretized form of G. Assuming exponential time dependence for G, $G(x,t)=\Phi(x)\exp(\beta t)$, yields the eigenvalue problem $\beta\mathbf{\Phi}=\mathbf{A}\mathbf{\Phi}$. For each value of the wave number q, the n eigenvalues of the matrix $\mathbf{A}$, $\beta_n(q)$, were found using the MATLAB 6.1 function *eig*. The domain length $L=L_1+L_2$ was chosen sufficiently large that β and Φ for the leading discrete and continuous mode do not change upon a further increase in L. It was found that $L_1=L_2=40$ is sufficient for β. The tails of the discrete eigenfunctions decay slowly as $x\to\infty$, particularly for $\{q_0:\beta(q_0)\approx-q_0^4\}$. It was found that the portion of the eigenfunction within the computational domain typically does not change away from the boundary for $L_2\geq40$. A very large computational domain ($L_2=400$) was used for the energy analysis so that the decaying tails of the discrete eigenfunctions are captured by extending the base state with its asymptotic behavior as $x\to\infty$ (h_{0xxx}, S_{xxx}, $T_x^i\to0$, $h_0\to1$). Other plots correspond to $L_1=40$ and $L_2=60$ unless noted otherwise.

III. RESULTS

Attention in this work is focused on step-down and mound topographies. The step-down topography is modeled as $S^{\text{I}}(x)=D\{0.5-\tan^{-1}[(x-a)/\delta]\}/\pi$, where D is the amplitude of the feature, δ determines its steepness, and a specifies the location of the feature. The mound topography is modeled as $S^{\text{II}}(x)=D\{\tan^{-1}[(x+w_1)/\delta]-\tan^{-1}[(x-w)/\delta]\}/\pi$. The width of the feature in the streamwise direction is $w+w_1$, and $w_1=0$ in the results that follow unless noted otherwise. Rep-

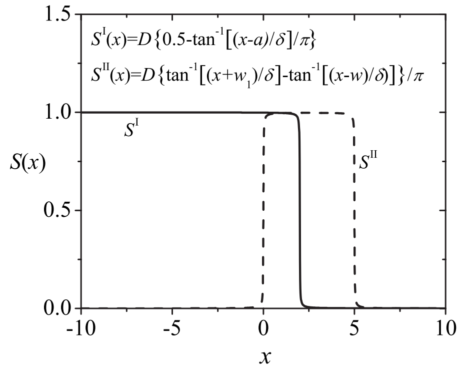

FIG. 2. Representative step-down (S^{I}) and mound (S^{II}) topographies with $D=1$, $\delta=0.01$, $a=2$, $w=5$, and $w_1=0$.

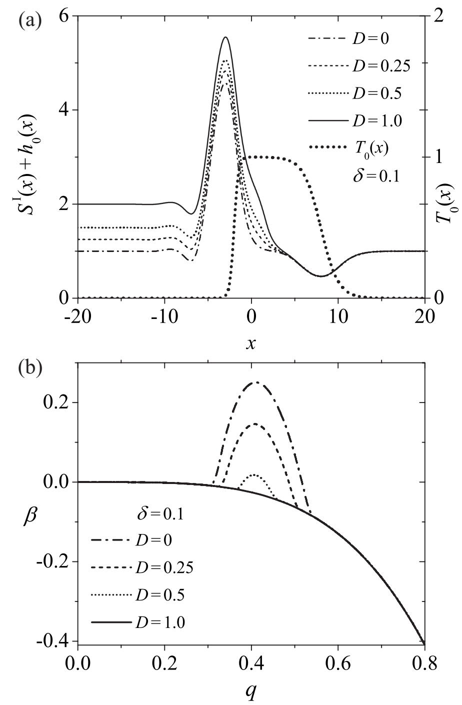

FIG. 3. (a) Effect of the amplitude D of the step-down topography S^{I} with $\delta=0.1$ and $a=2$ on the steady base profile for $M=17$, Bi$=0.01$, and $\omega=2$. The ordinate is the film thickness plus the height of the topographical feature. The substrate temperature T_0 is superimposed. (b) Corresponding dispersion curves. The computational domain is $-40\leq x\leq 60$.

resentative features are plotted in Fig. 2. The influence of D and δ on the shape of the steady base profiles of liquid films flowing over various features has been investigated extensively for isothermal flows using lubrication theory.[39] It has been shown that the height of the capillary ridge induced by the feature asymptotes to a constant value as $\delta\rightarrow 0$. A detailed investigation of liquid films flowing over locally heated flat surfaces based on Eqs. (3) and (6) has been the focus of previous studies,[24–26] including base profiles, linear stability analysis, and computations of the non-modal and nonlinear dynamics. Also discussed in these studies are comparisons of the base states and dispersion curves based on the model used here for flat surfaces to those computed in previous studies[20,21] that differ primarily in the choice of boundary conditions for the linear stability analysis, the temperature profile, and some parameter values.

A. Base profiles and linear stability

Base profiles of a liquid film flowing over a locally heated substrate with the step-down topography S^{I} are shown in Fig. 3(a) for $M=17$, Bi$=0.01$, $\omega=2$, $\delta=0.1$, and $a=2$. The surface is one unit below the film far from the step and the heater. The apparent amplitude of the thermocapillary ridge increases as D increases because the substrate below the ridge is raised. The most important influence of the topography on the film profile is the deformation of the downstream edge of the fluid ridge near $x=2$ due to the capillary pressure gradient induced by the step-down, and the deformation becomes more significant as D increases for fixed δ.

The stabilizing influence of the topography on the film is evident from the dispersion curves shown in Fig. 3(b) from a linear stability analysis of the profile in Fig. 3(a). As the height of the step-down increases, the largest eigenvalue decreases, and the width of the band of unstable wave numbers also decreases. The film is stable for $D=1$, and the dispersion relation is that for the continuous spectrum corresponding to decaying capillary waves. If D is increased above a critical value D_{c1}, the film is linearly stable, with a narrow band of discrete modes. If D is increased above a second critical value $D_{c2}>D_{c1}$, discrete modes cannot be found, and the stable continuous spectrum governs the dynamics of perturbations. Analogous behavior occurs for a flat substrate if M is decreased.[24,25] Discrete modes are similarly absent for relevant q for isothermal flows over topography.[40,41]

The effect of varying the steepness δ of the topography S^{I} on the film profile and its linear stability is shown in Fig. 4 for $M=17$, Bi$=0.01$, $D=1$, and $a=2$. The change in the base profile as δ is decreased is small and is restricted to the region around the center of the step-down at $x=2$. The change in the film's curvature is, however, sufficient to stabilize the flow. As δ is decreased the step-down becomes steeper, which generates a stronger capillary pressure gradient that apparently acts to suppress rivulet formation at the downstream edge of the capillary ridge. A band of stable discrete modes is apparent for $\delta=0.5$. For $\delta=0.1$ and steeper features, the band of discrete modes vanishes, and the film is linearly stable. The dispersion relation is that of the continuous spectrum, $\beta=-q^4$, as for isothermal flows over topography.[40,41] There are critical values δ_{c1} and δ_{c2} analogous to D_{c1} and D_{c2}.

Topographical features of finite width also have a stabilizing effect on the flowing film. Base profiles of thin liquid films flowing over a locally heated surface with the mound topography S^{II} are shown in Fig. 5(a) for $M=17$, Bi$=0.01$, $\omega=2$, $\delta=0.1$, and $w=5$. The influence of the topography on the base profile is pronounced for $0\leq x\leq 5$, as the film must flow over the mound, and the curvature of the film is modified significantly in this region. The corresponding dispersion curves are shown in Fig. 5(b), and the trend is similar to that for the step-down feature. As D is increased the maximum eigenvalue decreases, and the film is linearly stable for $D=1$.

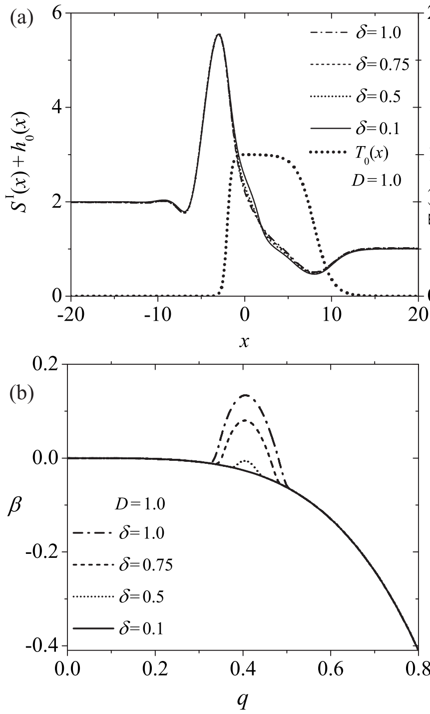

FIG. 4. (a) Effect of the steepness δ of the step-down topography S^{I} with $D=1.0$ and $a=2$ on the steady base profile for $M=17$, $\mathrm{Bi}=0.01$, and $\omega=2$. (b) Corresponding dispersion curves. The computational domain is $-40 \leq x \leq 60$.

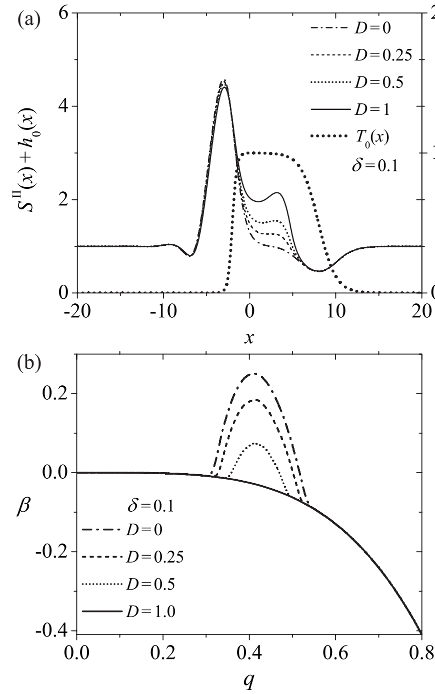

FIG. 5. (a) Effect of the amplitude D of the mound topography S^{II} with $\delta=0.1$ and $w=5$ on the steady base profile for $M=17$, $\mathrm{Bi}=0$, and $\omega=2$. (b) Corresponding dispersion curves. The computational domain is $-40 \leq x \leq 60$.

Shown in Fig. 6(a) are the base profiles for the flow when the steepness of the mound is changed while keeping the amplitude fixed at $D=1.0$ and other parameters as for Fig. 5. The corresponding dispersion curves are shown in Fig. 6(b), and the trend is similar to that for the step-down topography. As the mound becomes steeper the largest eigenvalue decreases. The step-down topography is more effective at stabilizing the flow than the mound topography for the parameters considered, as the film can be made linearly stable by a smaller or less steep feature. For example, the film is stable for a step-down feature with $D=1$ and $\delta=0.5$, but the film is unstable for a mound feature with the same D and δ. It was found, however, that the mound topography is effective for the larger values of Bi and steeper temperature increase considered in Fig. 7.

Trench features, which can be modeled as $S^{\mathrm{III}}=D-S^{\mathrm{II}}$, are typically not as effective at stabilizing the film as step-down or mound features for the ranges of M and D considered, and results are not shown. For relatively narrow trenches, the stabilization is found to increase with the feature width. As the width of the trench is increased to $w>10$, however, the dispersion curves are only weakly influenced by the width of the trench, and the feature essentially acts as an isolated step-down.

Results for different topographical features and various parameter values are summarized in plots of the critical Marangoni number M_c above which the film is unstable versus the Biot number. It has been shown[25] that for a flat substrate the amplitude of the thermocapillary ridge decreases as Bi increases because the interfacial temperature and its gradient are decreasing functions of Bi. In Figs. 7(a) and 7(b) it is evident that M_c decreases as Bi increases. For the small values of Bi that are of interest, $\mathrm{Bi} \leq 0.2$, the variation in the interfacial temperature induced by a perturbation, T_1^i, increases with Bi, so the transverse thermocapillary flow induced by a sinusoidal perturbation to the film increases with Bi. It has been shown from an energy analysis[20] that this transverse flow becomes a significant destabilizing mechanism as Bi increases, which explains the decrease in M_c with increasing Bi.

The results shown in Fig. 7(a) for the increase in M_c upon addition of the step-down topography S^{I} are similar to those shown in Fig. 7(b) for the mound topography S^{II}. At $\mathrm{Bi}=0$, M_c increases by approximately 25% as the amplitude of the topography is increased from $D=0$ to $D=1$. At $\mathrm{Bi}=0.1$, the increase in M_c is reduced to approximately 13%. This stabilization is significant given the relatively blunt topographical features that have been used.

Steeper features generate larger capillary pressure gradients and thus are expected to have a more impressive stabilizing influence on the film. Results for the steeper mound S^{II} with $D=1$, $w=5$, and $\delta=0.02$ are shown in Fig. 7(c). The temperature increase at the heater is also sharper with $\omega=3.5$, which corresponds to a more unstable film with a significantly lower M_c on a flat surface.[25] The stabilization induced by this steeper topography is significant, as M_c is increased by a factor of 1.7 for $\mathrm{Bi}=0.08$ and nearly a factor of 4 for $\mathrm{Bi}=0.04$. For smaller Biot numbers, $\mathrm{Bi}<0.02$, the film was stable with the topography even for extremely large values of M $(M>70)$ that correspond to a ridge amplitude nearly an order of magnitude larger than the film thickness before the heater. The dominant instability mechanisms for

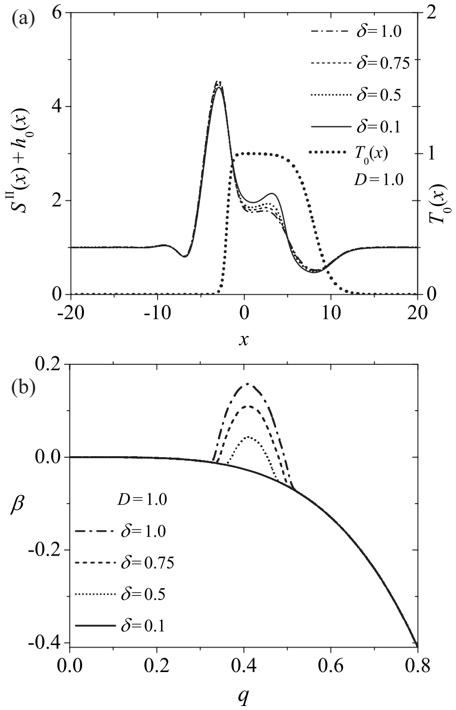

FIG. 6. (a) Effect of the steepness δ of the mound topography S^{II} with $D=1.0$ and $w=5$ on the base profile for $M=17$, and $\mathrm{Bi}=0.01$, and $\omega=2$. (b) Corresponding dispersion curves. The computational domain is $-40 \leq x \leq 60$.

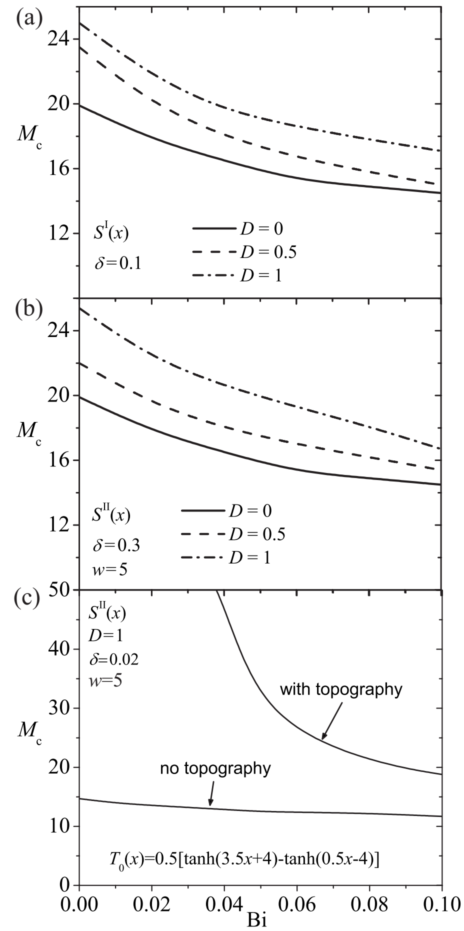

FIG. 7. Effect of Bi on M_c for flow over (a) S^I and (b) S^{II} with varying D and $\omega=1$. (c) Effect of steeper topography S^{II} with $\delta=0.02$ and $D=1.0$ on a film flowing over a substrate with a sharper temperature increase with $\omega=3.5$.

small Bi are gravity and the capillary pressure gradient induced by the thermocapillary ridge,[24] and the restoring flow generated by the topography is evidently sufficient to overcome these destabilizing mechanisms. The stabilization is even more pronounced for less abrupt temperature increases at the heater ($\omega=1$). An energy analysis of the governing linear operator corresponding to **A** is presented in Sec. III B to provide further insight into the physical mechanisms by which the topography stabilizes the flow.

The "optimal" topography that entirely suppresses the distortion of the free surface induced by the Marangoni stress can be found from an extension of the study of Sellier[53] to nonisothermal flows. Letting $H(x) \equiv h_0(x)+S(x)$, Eq. (7) for the shape of the steady base state becomes

$$[H(x)-S(x)]^3(H_{xxx}+1) = MT_x^i[H(x)-S(x)]^2+1. \qquad (12)$$

With $H(x)$ specified as the desired shape of the free surface, Eq. (12) can be solved to determine the topography $S(x)$ that yields the desired film profile. For example, if a flat interface is desired, with $H=1$, $H_{xxx}=0$, and in the limit $\mathrm{Bi} \to 0$, Eq. (12) reduces to $(1-S)^3 - MT_{0x}(1-S)^2 - 1 = 0$, which is a simple polynomial for the substrate shape $S(x)$. This technique is illustrated for the case of $M=10$, $\mathrm{Bi}=0$, and $\omega=1$. Plotted in Fig. 8(a) are the interfacial temperature $T_0(x)$ and the film profile without topography, $h_0(x)$. The optimal topography $S(x)$ required to produce a flat interface, $H(x) \equiv h_0(x)+S(x)=1$, is plotted in Fig. 8(b) along with the computed $H(x)$ with this optimal topography. While the optimal topography yields a perfectly flat gas-liquid interface even with the Marangoni stress at the heater, it is of rather limited utility. The optimal topography must be computed for each temperature profile $T_0(x)$, and the required feature for larger M is very deep. This study demonstrates, however, that the topography that has the most substantial influence on the thermocapillary ridge has a significant feature where $|MT_x^i|$ is maximized. The step-down and mound features that are investigated more extensively in this work are of smaller amplitude, would be simpler to fabricate, and are effective for different film thicknesses and temperature profiles. A similar procedure can be used to determine the optimal $T^i(x)$ to suppress the ridge induced by a given topographical feature $S(x)$.

B. Energy analysis

An energy analysis is performed to explore the mechanism associated with the stabilization of the thermocapillary ridge by topographical features. Following Spaid and Homsy,[30] the exponential growth rate characterized by the eigenvalue β is interpreted as a rate of energy production, $\dot{E}$. This result follows by defining the mechanical energy associated with the disturbance Φ as $E=0.5\int_{-\infty}^{+\infty}\Phi\bar{\Phi}dx$, differentiating with respect to time, and taking the inner product of Eq. (8) with Φ. The contributions of the individual terms in the disturbance operator $\mathbb{L}$ to $\dot{E}$ can be isolated to infer the

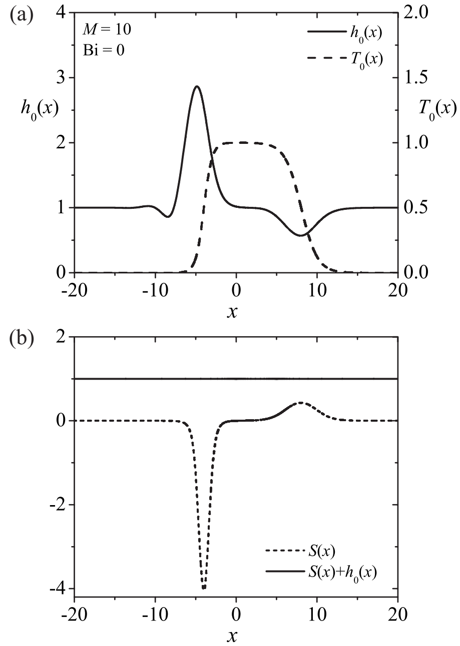

FIG. 8. (a) Film profile $h_0(x)$ and interfacial temperature $T_0(x)$ for flow over a flat substrate with $M=10$. (b) Optimal topographical feature $S(x)$ that produces a uniform free-surface $h_0+S=1$ even with localized heating.

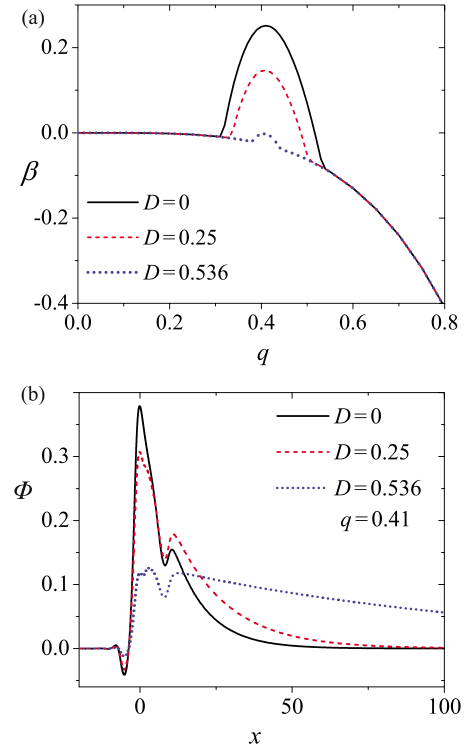

FIG. 9. (Color online) (a) Dispersion curves for $M=17$, Bi=0.01, $\omega=2$, and topography S^{I} with $\delta=0.1$ and $a=2$ for $D=0$ (unstable), $D=0.25$ (unstable), and $D=0.536$ (linearly stable). There is a band of stable discrete modes corresponding to $0.39 \leq q \leq 0.43$ for $D=0.536$. (b) Eigenfunctions corresponding to the leading (least stable) eigenvalue for $q=0.41$ for different feature heights to illustrate the slow decay as $x \to \infty$. The computational domain is $-40 \leq x \leq 400$.

influence of various physical mechanisms on the growth or decay of perturbations. The terms in Eq. (8) make contributions $\dot{E}_n$ to $\dot{E}$, which can be found from[30]

$$\dot{E}_n = \frac{\langle \mathbf{\Phi}, \mathcal{L}_n \mathbf{\Phi} \rangle}{\langle \mathbf{\Phi}, \mathbf{\Phi} \rangle}, \tag{13}$$

where $\langle \cdot , \cdot \rangle$ represents the inner product, which is taken to be a finite integral over the computational domain. The energy analysis is applied to the base profiles examined in Figs. 3 and 4 that correspond to $M=17$, $\omega=2$, Bi=0.01, and topography S^{I} with $a=2$ and three values of D. As shown in Fig. 9(a), the film is unstable for $D=0$ and $D=0.25$. The film is linearly stable for $D=0.536$, and there is a band of discrete modes for $0.39 \leq 0.43$. Eigenfunctions for $q=0.41$, which corresponds to the leading eigenvalue, are shown in Fig. 9(b). The distance required for the eigenfunction to decay as $x \to \infty$ increases significantly as D increases. While a computational domain that is smaller than the distance required for the eigenfunction to decay to zero was found to have a minimal influence on the dispersion curves and the shape of the eigenfunction within the domain, such a shorter domain strongly influences the energy analysis. The computational domain used for Figs. 9–12 is therefore $-40 \leq x \leq 400$, which captures the decay of the discrete eigenfunctions as $x \to \infty$. It was verified that further increases in the domain length have no influence on the energy analysis results for the discrete modes. The results for continuous modes do however change with domain length because the eigenfunctions have spatial variations only in the vicinity of the heater and topography, and the constant values as $x \to \pm\infty$ make larger contributions to the inner product as the domain length increases. This change is small for the large domain considered however, and the emphasis of this study is on the discrete modes that are associated with instability.

Each $\mathcal{L}_n$ is a group of terms in $\mathbb{L}$ listed in Table I along with its physical meaning. These terms depend nonlinearly on the base flow solution, $h_0(x)$, and perturbation wave number, q. Terms that make a negative energy contribution are stabilizing, while terms corresponding to a positive $\dot{E}_n$ are destabilizing. Noting that $\mathbb{L}=\Sigma\mathcal{L}_n$, it follows from Eq. (13) that $\Sigma\dot{E}_n=\beta$.

Results of the classical energy analysis are shown in Fig. 10. The original interpretation of the energy analysis for spreading films[30–32] was subsequently improved[20,33] by considering not the absolute energy production rates of various terms but instead the deviation of the energy gains relative to their values for the transversely invariant, neutrally stable mode, $\dot{E}_n(q)-\dot{E}_n(q=0)$. This updated interpretation was shown[20] to give consistent results for prior studies.[31,32] While the relevance of this new interpretation to the present problem is less clear because the neutrally stable mode for $q=0$ is continuous and the unstable modes are discrete, using this enhanced interpretation does not qualitatively alter the results shown in Fig. 10 because the $\dot{E}_n$ for the discrete modes is much larger in magnitude than for the mode corresponding to $q=0$.

For the flat substrate with $D=0$, examination of $\dot{E}_n(q) - \dot{E}_n(q=0)$ reveals that the dominant destabilizing mecha-

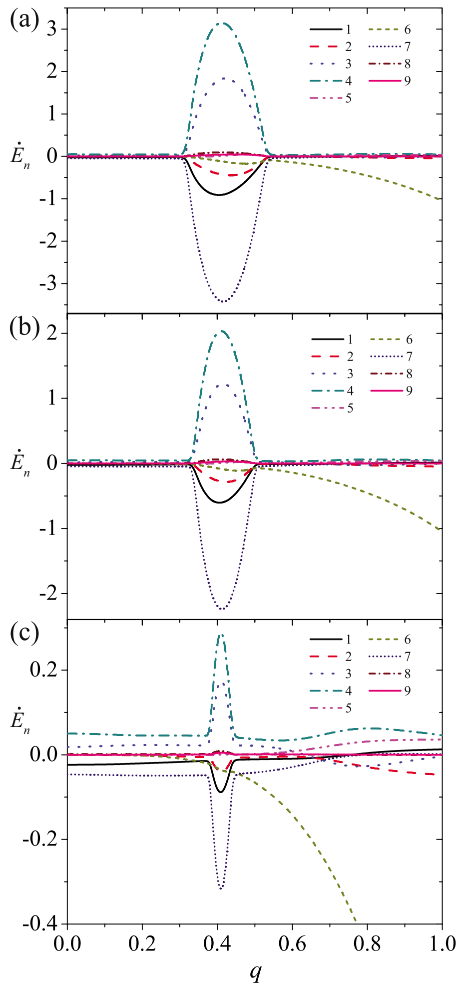

FIG. 10. (Color online) Energy production rate $\dot{E}_n$ of the individual terms of the governing linear operator listed in Table I for the film with $M=17$, $\mathrm{Bi}=0.01$, $\omega=2$, $a=2$, and (a) $D=0$, (b) $D=0.25$, and (c) $D=0.536$.

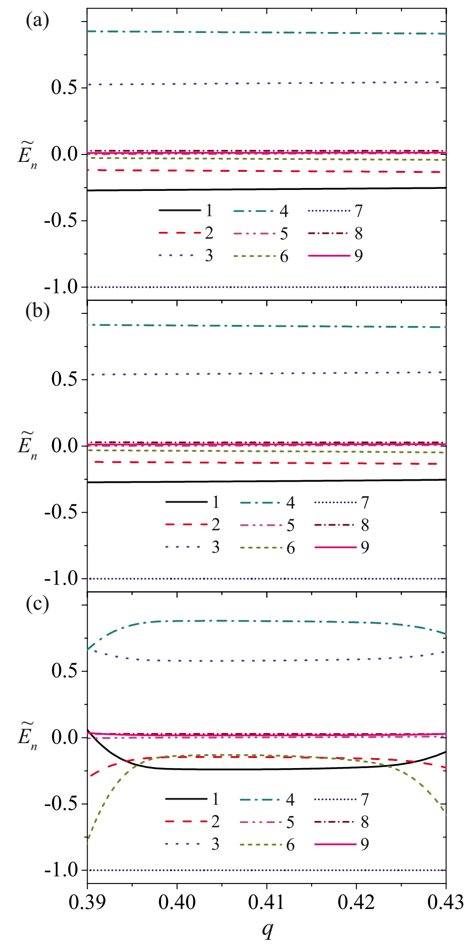

FIG. 11. (Color online) Energy production rate relative to that for the neutrally stable, transversely invariant mode with $q=0$ and normalized by the magnitude of the rate for term 7 (dominant Marangoni term): $\tilde{E}_n(q)=[\dot{E}_n(q)-\dot{E}_n(q=0)]/|\dot{E}_7(q)-\dot{E}_7(q=0)|$. (a) $D=0$. (b) $D=0.25$. (c) $D=0.536$.

nism is term 4, which corresponds to flow in the x-direction due to the streamwise curvature of the film. Term 3, which represents flow in the x-direction due to gravity, is also significantly destabilizing. This mechanism corresponds to mobility differences in the film, as locally thicker regions have less resistance to flow under the influence of gravity (or other body force) than locally thinner regions. Term 7, which corresponds to thermocapillary flow in the x-direction due to the influence of the base state's Marangoni stress on the perturbation, is strongly stabilizing. It is important to note, however, that this Marangoni stress is responsible for the formation of the thermocapillary ridge that ultimately leads to instability, which reflects the care needed to interpret the results of the energy analysis in spatially nonuniform films for which different physical mechanisms can be nonlinearly coupled through the base state. Other notable stabilization results from terms 1, 2, and 6. These results for the flat substrate are in complete agreement with those of Skotheim *et al.*[20] for $\mathrm{Bi}\to 0$.

The results of the energy analysis for $D=0.25$ are qualitatively similar, but the magnitude of the contributions from the various terms decreases for the discrete modes because the film is less unstable. These contributions are further reduced in magnitude for $D=0.536$, which corresponds to a linearly stable film. The $\dot{E}_n$ from the continuous modes are more apparent in Fig. 10(c), although these values typically do not deviate significantly from their values at $q=0$, and again $\dot{E}_n(q)-\dot{E}_n(q=0)$ is the relevant quantity. For the discrete modes corresponding to $0.39\leq 0.43$ for $D=0.536$, terms 3 and 4 are destabilizing, and terms 1, 2, 6, and 7 are

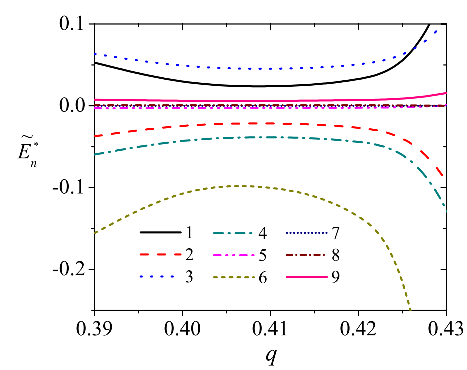

FIG. 12. (Color online) Change in the normalized energy production rate of each term in Fig. 11 from $D=0$ to $D=0.536$: $\tilde{E}_n^*=\tilde{E}_n(D=0.536)-\tilde{E}_n(D=0)$.

TABLE I. Terms comprising the governing linear operator from the stability problem along with the physical interpretation of each term.

Term	Expression	Physical meaning
1	$-(h_0^3 h_{1xxx})_x$	Capillary flow in x-direction induced by perturbation curvature variation in x
2	$q^2(h_0^3 h_{1x})_x$	Capillary flow in x-direction due to streamwise change in transverse perturbation curvature
3	$-3(h_0^2 h_1)_x$	Flow in x-direction due to gravity
4	$-3[h_0^2(h_{0xxx}+S_{xxx})h_1]_x$	Capillary flow in x-direction driven by the base-state capillary pressure gradient acting on the perturbation
5	$q^2 h_0^3 h_{1xx}$	Capillary flow in y-direction induced by perturbation curvature in x
6	$-q^4 h_0^3 h_1$	Capillary flow in y-direction induced by perturbation curvature in y
7	$M(T_{0x}^i h_0 h_1)_x$	Thermocapillary flow in x-direction due to perturbation thickness variations
8	$M(h_0^2(T_1^i h_1)_x)_x$	Thermocapillary flow in x-direction due to streamwise temperature variations
9	$-q^2 M h_0^2 T_1^i h_1$	Thermocapillary flow in y-direction due to transverse temperature gradients

the most significant stabilizing terms, as for the unstable film with $D=0$. Aside from the reduced magnitude of each $\dot{E}_n$, the primary difference is that term 6 makes a more significant relative contribution for the stable film. The significant change in the magnitude of each $\dot{E}_n$ with D for the discrete modes occurs because a change in the parameter D alters both the base state $h_0(x)$, through which the different physical mechanisms influencing the film are nonlinearly coupled and which determines $\mathcal{L}_n$ for the spatially nonuniform film and the shape of the eigenfunction Φ.

Direct comparison of the $\dot{E}_n$ for different D cannot be made to gain insight into the stabilization mechanism from topography because the contributions of the key terms vary by an order of magnitude from Figs. 10(a)–10(c). Instead, the contribution of each term can be normalized by the magnitude of term 7 to facilitate a comparison for the discrete modes that are associated with instability. Plotted in Fig. 11 is $\tilde{E}_n(q)$ versus q, where $\tilde{E}_n=[\dot{E}_n(q)-\dot{E}_n(q=0)]/|\dot{E}_7(q)-\dot{E}_7(q=0)|$, for the interval $0.39\leq q\leq 0.43$, which corresponds to discrete modes for each D in Fig. 10. With this normalization, the results for the unstable films with $D=0$ and $D=0.25$ appear nearly identical for the most unstable discrete modes. The results for the stable film with $D=0.536$ are qualitatively similar, but the most pronounced difference is that term 6 is significantly more stabilizing. This relative change in term 6 as D is increased is larger than for any other term, as is apparent in Fig. 12, in which $\tilde{E}_n^* \equiv \tilde{E}_n(D=0.536)-\tilde{E}_n(D=0)$ is plotted versus q. The increased stabilization of term 6 for the discrete modes can be interpreted based on the shape of the eigenfunctions shown in Fig. 9(b). As D is increased, the discrete mode decays more slowly as $x\to\infty$ and tends toward the shape of the continuous mode that is constant and nonzero away from the heater and topography. Far from the heater, $h_0\to 1$, $T_{0x}^i\to 0$, $T_0\to 0$, and $T^i\to 0$. Consequently, there is very little contribution to most terms in Table I from the region of the domain far downstream of the heater at which $\Phi\neq 0$. Term 6, however, simplifies to $-q^4\Phi$ downstream of the heater, and the contribution of this term increases with the size of the decaying tail of the eigenfunction. The stabilizing effect of topography can therefore be interpreted based on its influence on the shape of the eigenfunction, which increases the contribution of the restoring capillary flow in the y-direction from the transverse curvature of the perturbation. This stabilizing mechanism is identical to that for a flat isothermal film, as is seen by considering the trivial case with $h_0=1$ and $T_0=S=0$.

IV. CONCLUSION

The influence of topographical features on the linear stability of thin liquid films flowing over locally heated surfaces was considered using a long-wave lubrication analysis. Simple step-down and mound features were found to stabilize the film effectively, as the critical Marangoni number M_c at the instability threshold increases substantially with appropriate topography even for nonzero Biot numbers. Steep topographical features were found to increase M_c by more than a factor of four for small Bi. The optimal topographical features that suppress all variation in the shape of the free surface due to the thermocapillary flow were also determined. While the generality of these results may be restricted somewhat by the limitations of the lubrication analysis, it has previously been shown that the results of lubrication theory are in good agreement with boundary integral computations of the unsimplified Stokes equations for the flow of an isothermal film over topography for small capillary numbers ($\mathrm{Ca}<0.01$), even for very steep topographical features.[42] Finite element solutions[43] of the full Navier–Stokes equations further confirm the accuracy of the lubrication solutions in this regime even though some of the restrictions inherent to the reduction in dimensionality of lubrication theory are not entirely satisfied. The results presented here are therefore expected to be valid for such small capillary numbers that correspond to thin films. For larger Ca, the liquid film follows the topographical feature more closely with a negligible capillary ridge.[42] It would be interesting in future work to extend the present study to larger Ca for which the lubrication analysis is not valid, to the regime in which convective heat transport in the flowing film is significant, and to direct numerical simulation of the unsimplified momentum and energy equations.

An energy analysis was used to provide insight into the mechanism by which the topography stabilizes the flow. While the streamwise gradient in the capillary pressure is the expected stabilization mechanism because it is strongly stabilizing for isothermal flow over topography, this term is destabilizing for topographical features on the locally heated surface. Upon the addition of topography, stabilization is primarily due to the influence of the topography on the shape of the leading eigenfunction, which enhances the restoring capillary flow from the transverse curvature of the perturbation. Additional energy damping occurs from the influence of the topography on the steady base state, through which the various physical mechanisms in the energy analysis are nonlinearly coupled.

The strong stabilization from topography contrasts with its influence on liquid films resting on heated horizontal surfaces. For this configuration topography was shown to make the films less stable to long-wave disturbances relative to flat surfaces.[3] The contrasting effects of the topography occur because of differences in the dominant instability mechanisms in the two cases. For the horizontal surface, instability occurs because of a thermocapillary flow due to temperature variations along the interface, and these variations are enhanced by the topography. For the film flowing over a locally heated surface, the instability is primarily due to mobility differences and variations in the film curvature associated with the fluid ridge that forms upstream of the heater. Topographical features at the downstream edge of this ridge modify the film profile and curvature, which significantly stabilizes the film. Because the stabilizing effect of sufficiently steep topographical features is only weakly sensitive to the governing parameters and particular temperature profile, the use of such features could be a simple alternative to more complicated methods of stabilization in some applications involving nonuniform heating.

ACKNOWLEDGMENTS

J.M.D. kindly acknowledges support from NSF (Award No. CBET-0644777) and the Camille Dreyfus Teacher-Scholar Awards Program.

[1] S. H. Davis, "Thermocapillary instabilities," Annu. Rev. Fluid Mech. **19**, 403 (1987).
[2] A. Oron, S. H. Davis, and S. G. Bankoff, "Long-scale evolution of thin liquid films," Rev. Mod. Phys. **69**, 931 (1997).
[3] Y. O. Kabova, A. Alexeev, T. Gambaryan-Roisman, and P. Stephan, "Marangoni-induced deformation and rupture of a liquid film on a heated microstructured wall," Phys. Fluids **18**, 012104 (2006).
[4] C. M. Gramlich, S. Kalliadasis, G. M. Homsy, and C. Messer, "Optimal leveling of flow over one-dimensional topography by Marangoni stresses," Phys. Fluids **14**, 1841 (2002).
[5] D. L. DeVoe, "Thermal issues in MEMS and microscale systems," IEEE Trans. Compon. Packag. Technol. **25**, 576 (2002).
[6] S. Lin, "Finite amplitude side-band instability of a viscous film," J. Fluid Mech. **63**, 417 (1974).
[7] S. Sreenivasan and S. P. Lin, "Surface tension driven instability of a liquid film flowing down a heated incline," Int. J. Heat Mass Transfer **21**, 1517 (1978).
[8] R. Kelley, S. Davis, and D. Goussis, "On the instability of a heated film flow with variable surface tension," *Proceedings of the Eight International Heat Transfer Conference*, San Francisco, CA (A87-30676 12-34) (Hemisphere, Washington, DC, 1986), Vol. 4, p. 1937.
[9] A. A. Darhuber, J. M. Davis, S. M. Troian, and W. W. Reisner, "Thermocapillary actuation of liquid flow on chemically patterned surfaces," Phys. Fluids **15**, 1295 (2003).
[10] A. A. Darhuber, J. P. Valentino, J. M. Davis, S. M. Troian, and S. Wagner, "Fluidic actuation with addressable microheater arrays," Appl. Phys. Lett. **82**, 657 (2003).
[11] J. Davies and E. Rideal, *Interfacial Phenomena* (Academic, New York, 1963).
[12] J. R. Pearson, "On convection cells induced by surface tension," J. Fluid Mech. **4**, 489 (1958).
[13] C. V. Sternling and L. E. Scriven, "Interfacial turbulence: Hydrodynamic stability and the Marangoni effect," AIChE J. **5**, 514 (1959).
[14] S. W. Joo, S. H. Davis, and S. G. Bankoff, "Long wave instabilities of heated films: Two dimensional theory of uniform layers," J. Fluid Mech. **230**, 117 (1991).
[15] B. Scheid, C. Ruyer-Quil, U. Thiele, O. A. Kabov, J. C. Legros, and P. Colinet, "Validity domain of the Benney equation including the Marangoni effect for closed and open flows," J. Fluid Mech. **527**, 303 (2005).
[16] A. Oron and P. Rosenau, "On a nonlinear thermocapillary effect in thin liquid layers," J. Fluid Mech. **273**, 361 (1994).
[17] U. Thiele and E. Knobloch, "Thin liquid films on a slightly inclined heated plate," Physica D **190**, 213 (2004).
[18] W. Boos and A. Thess, "Cascade of structures in long-wavelength Marangoni instability," Phys. Fluids **11**, 1484 (1999).
[19] B. Scheid, A. Oron, P. Colinet, U. Thiele, and J. C. Legros, "Nonlinear evolution of nonuniformly heated falling liquid films," Phys. Fluids **14**, 4130 (2002).
[20] J. M. Skotheim, U. Thiele, and B. Scheid, "On the instability of a falling film to localized heating," J. Fluid Mech. **475**, 1 (2003).
[21] S. Kalliadasis, A. Kiyashko, and E. A. Demekhin, "Marangoni instability of a thin liquid film heated from below by a local heat source," J. Fluid Mech. **475**, 377 (2003).
[22] A. M. Frank, "3D numerical simulation of regular structure formation in a locally heated falling film," Eur. J. Mech. B/Fluids **22**, 445 (2003).
[23] A. M. Frank and O. A. Kabov, "Thermocapillary structure formation in a falling film: Experiment and calculations," Phys. Fluids **18**, 032107 (2006).
[24] N. Tiwari, Z. Mester, and J. M. Davis, "Linear stability and transient dynamics of non-inertial coating flows over locally heated surfaces," Phys. Rev. E **76**, 056306 (2007).
[25] N. Tiwari and J. M. Davis, "Linear stability of a volatile liquid film flowing over a locally heated surface," Phys. Fluids **21**, 022105 (2009).
[26] N. Tiwari and J. M. Davis, "Non-modal and nonlinear dynamics of a volatile liquid film flowing over a locally heated surface," Phys. Fluids **21**, 102101 (2009).
[27] O. A. Kabov, "Heat transfer from a small heater to a falling liquid film," Heat Transfer Res. **27**, 221 (1996).
[28] O. A. Kabov, "Formation of regular structures in a falling liquid film upon local heating," Thermophys. Aeromechanics **5**, 547 (1998).
[29] S. W. Joo, S. H. Davis, and S. G. Bankoff, "A mechanism for rivulet formation in heated films," J. Fluid Mech. **321**, 279 (1996).
[30] M. A. Spaid and G. M. Homsy, "Stability of Newtonian and viscoelastic dynamic contact lines," Phys. Fluids **8**, 460 (1996).
[31] D. E. Kataoka and S. M. Troian, "A theoretical study of instabilities at the advancing front of thermally driven coating films," J. Colloid Interface Sci. **192**, 350 (1997).
[32] D. E. Kataoka and S. M. Troian, "Stabilizing the advancing front of thermally driven climbing films," J. Colloid Interface Sci. **203**, 335 (1998).
[33] U. Thiele and E. Knobloch, "Front and back instability of a liquid film on a slightly inclined plate," Phys. Fluids **15**, 892 (2003).
[34] S. Kalliadasis, E. A. Demekhin, C. Ruyer-Quil, and M. G. Velarde, "Thermocapillary instability and wave formation on a film falling down a uniformly heated plane," J. Fluid Mech. **492**, 303 (2003).
[35] A. M. Frank, "Suppression of thermocapillary instability in a falling film," Phys. Fluids **18**, 078106 (2006).

[36]E. A. Demekhin, S. Kalliadasis, and M. G. Velarde, "Suppressing falling film instabilities by Marangoni forces," Phys. Fluids **18**, 042111 (2006).
[37]L. E. Stillwagon and R. G. Larson, "Fundamentals of topographic substrate leveling," J. Appl. Phys. **63**, 5251 (1988).
[38]L. E. Stillwagon and R. G. Larson, "Leveling of thin films over uneven substrates during spin coating," Phys. Fluids A **2**, 1937 (1990).
[39]S. Kalliadasis, C. Bielarz, and G. M. Homsy, "Steady free-surface thin film flow over two-dimensional topography," Phys. Fluids **12**, 1889 (2000).
[40]S. Kalliadasis and G. M. Homsy, "Stability of free-surface thin-film flows over topography," J. Fluid Mech. **448**, 387 (2001).
[41]J. M. Davis and S. M. Troian, "Generalized linear stability of noninertial coating flows over topographical features," Phys. Fluids **17**, 072103 (2005).
[42]A. Mazouchi and G. M. Homsy, "Free surface Stokes flow over topography," Phys. Fluids **13**, 2751 (2001).
[43]P. H. Gaskell, P. K. Jimack, M. Sellier, H. M. Thompson, and M. C. T. Wilson, "Gravity-driven flow of continuous liquid films on non-porous substrates with topography," J. Fluid Mech. **509**, 253 (2004).
[44]M. M. J. Decré and J.-C. Baret, "Gravity-driven flows of viscous liquids over two-dimensional topographies," J. Fluid Mech. **487**, 147 (2003).
[45]T. Gambaryan-Roisman and P. Stephan, "Flow and stability of rivulets on heated surfaces with topography," ASME Trans. J. Heat Transfer **131**, 033101 (2009).
[46]K. Helbig, R. Nasarek, T. Gambaryan-Roisman, and P. Stephan, "Effect of longitudinal minigrooves on flow stability and wave characteristics of falling liquid films," ASME Trans. J. Heat Transfer **131**, 011601 (2009).
[47]S. Saprykin, P. M. J. Trevelyan, R. J. Koopmans, and S. Kalliadasis, "Free-surface thin-films over uniformly heated topography," Phys. Rev. E **75**, 026306 (2007).
[48]P. Deuflhard, "A modified Newton method for the solution of ill-conditioned systems of nonlinear equations with application to multiple shooting," Numer. Math. **22**, 289 (1974).
[49]P. Deuflhard, "A stepsize control for continuation methods and its special application to multiple shooting techniques," Numer. Math. **33**, 115 (1979).
[50]W. E. Schiesser, *The Numerical Method of Lines* (Academic, San Diego, 1991).
[51]K. E. Brennan, S. L. Campbell, and L. R. Petzold, *Numerical Solution of Initial-Value Problems in Differential-Algebraic Equations* (Elsevier, New York, 1989).
[52]P. N. Brown, A. C. Hindmarch, and L. R. Petzoid, "Using Krylov methods in the solution of large-scale differential-algebraic systems," SIAM J. Sci. Comput. (USA) **15**, 1467 (1994).
[53]M. Sellier, "Substrate design or reconstruction from free surface data for thin film flows," Phys. Fluids **20**, 062106 (2008).